Supporting Information

Dynamics of prebiotic RNA reproduction illuminated by chemical game theory

J.A.M. Yeates, C. Hilbe, M. Zwick, M.A. Nowak, and N. Lehman

Contents:

Full Methods

Experimental Studies

RNA preparation

The **WXY** and **WXYZ** molecules, which are portions of the self-splicing group I intron from the isoleucine pre-tRNA in the purple bactierium *Azoarcus* (1), were prepared by *in-vitro* transcription from DNA plasmid templates. The **Z** fragment was purchased from TriLink Biotechnologies (San Diego, CA) and was gel purified prior to use. All RNAs were resuspended in 1–10 μM solutions in 0.1 mM EDTA. For quantification, < 0.1 μM of the **WXY**-fragment was 5′-labeled with γ[^{32}P]•ATP using OptiKinase (USB, Cleveland, OH).

Self-assembly kinetics (Quadrants **a** *and* **d** *of the payoff matrix)*

See Fig. 2 for a schematic of this process. Reaction mixtures containing **WXY** (1 μM), **Z** (1 μM), **WXYZ** (0 – 2 μM), and ^{32}P-labeled **WXY** (≤ 0.003 μM), all of the same IGS and tag genotype, were heated to 80 ˚C for 2 minutes then cooled to 48 ˚C. Time "zero" aliquots were drawn and quenched with equivolume quench solution (125 mM EDTA and 2X loading dye containing formamide and bromophenol blue). Reactions were initiated with the addition of reaction buffer (100 mM $MgCl_2$ and 30 mM EPPS, pH 7.5). Time point samples were drawn and immediately quenched with quench solution at 0.5, 1.0, 2.0, 5.0, 10, and 30 minutes. Samples were loaded on an 8% polyacrylamide/ 8M urea gel and **WXY** and **WXYZ** bands were separated. Visualization and quantification was possible *via* phosphorimaging on a Typhoon Trio+ variable mode phosphorimager (GE Healthcare) and accompanying ImageQuant software (GE Healthcare). A product ratio was calculated by comparing the RNA in the product **WXYZ** band to the unreacted **WXY** band (% reacted = [reacted / (reacted + unreacted)]*100%). Kinetic values were calculated as previously described (2). Briefly, initial rates were calculated from the slope of the linear portion of the reaction curve from a plot of the product ratio versus time (total of $n = 3$ trials for each concentration). For fast reactions this was ≤ 5 minutes and for slower reactions ≤ 10 minutes. The rate constant (k_a) was calculated from the slope of the initial **WXYZ** concentration versus the initial rate of the reaction (Fig. S1).

Kinetic parameter justification

The kinetic parameters of a ribozyme form of the *Azoarcus* group I intron have been studied by Kuo *et al.*, who demonstrated that the chemical step of *trans*-esterification was the rate-limiting process in this ribozyme (3). Previously we demonstrated that the full-length ribozyme **WXYZ**, can be broken into two (or three or four) fragments that could spontaneously self-assemble (2, 4) Self-assembly occurs when fragments hybridize through base-pairing (2˚) and tertiary (3˚) interactions to form non-covalent "*trans*" complexes of the ribozyme. Once formed, *trans* complexes can catalyze recombination reactions on other hybridized fragments (*i.e.*, **WXY** + **Z**) to synthesize covalent versions of the ribozyme. Recognition between a catalytic complex, either a *trans* complex or a fully covalently-contiguous ribozyme, is driven by the strength of the IGS-tag base pairing, as shown in Table 1 in Fig. S1 below. For example, the wildtype IGS in the *Azoarcus* ribozyme is 5′–GUG–3′, which *in vivo* matches with the pseudocomplement 5′–CAU–3′ as a consequence of a requisite G-U wobble preceding the splice site. A catalytic event creates a covalent closure of the stem-loop, often with the release of one or two G nucleotides from the 5′ end of the **Z** molecule GGCAU (ref. 24); thus this is a recombination reaction (5). In a population of molecules, this reaction is autocatalytic because the product (**WXYZ**) is a ribozyme that has an approximately 2-fold higher k_{cat} than the *trans* complex (2, 6).

In our system, RNA genotypes assemble one another from background material *via* kinetics that are driven by first order (or pseudo-first order) reactions; the units of the autocatalytic rate constants are per minute. In cases where molecules are being covalently formed from their own fragments, the initial rate has both autocatalytic (k_a) and non-autocatalytic (k_b) contributions: $(d[\mathbf{WXYZ}]/dt)_i = k_a[\mathbf{WXYZ}]^p + k_b$, where p represents a variable reaction order that must be experimentally determined (7)). We have previously shown that these self-assembly reactions display a high degree of autocatalytic rate enhancements, with autocatalytic efficiencies (the ratio of the slope to the y-intercept in the plots in Fig. S1 below) near the high end of such reported values (2). Although the exact value of the order (p) of the autocatalytic reaction is not straightforward, our modeling in ref. 2 suggests that a first-order ($p \sim 1$) fits the kinetic data very well, leading to units of min^{-1} in Table 1 below (Fig S1).

2-strategy kinetics (Quadrants* b *and* c *of the payoff matrix)
See Figs. 2*A*, 2*B*, and 2*C* for a schematic of this process. Reactions, visualization and quantitation were performed same as the self-assembly kinetics with the exception of the fragment genotypes. For the *b* quadrant, the initial mixture contained 1 μM of the player 2 genotype and a trace amount of ^{32}P-labeled **WXY** (≤ 0.003 μM) of the player 1 genotype. For the *c* quadrant, the initial mixture contained 1 μM of the player 1 genotype and a trace amount of ^{32}P-labeled **WXY** (≤ 0.003 μM) of the player 2 genotype.

Serial dilutions
A master mix reaction mixture was formed containing equimolar **WXY** genotype 1 (0.5 μM) and **WXY** genotype 2 (0.5 μM) and **Z** (1.0 μM). The mixture was then divided in two equal volumes. One part was doped with ^{32}P-labeled **WXY** genotype 1 and the other part with ^{32}P-labeled **WXY** genotype 2. The two reaction mixtures were then aliquoted into eight tubes each (one for each burst). (In the case of AU *vs*. UC, the original master mix made for the eight bursts was made at a 20:80, 50:50, or 05:95 ratio, and then divided into eight portions, and then this was used as above. See Fig. S2.) All tubes were heated up to 80 ˚C for 2 minutes and then cooled to 48 ˚C. The reaction in the first tube was initiated with the addition of reaction buffer (100 mM $MgCl_2$ and 30 mM EPPS, pH 7.5). At 5 minutes, 10% of the solution volume from tube #1 was transferred to tube #2, and tube #1 was placed on ice. Reaction buffer was immediately added to tube #2 while tube #1 was subsequently quenched with equal volume of quench solution. The transfer protocol was repeated through eight bursts. The two-part master mix containing ^{32}P-labeled **WXY** was used as a negative control for the assay. Gel separation, visualization and quantitation was performed same as kinetic assays. Three-strategy serial dilutions (Fig. 4*A*) were performed using the same protocol as above with the addition of a third genotype.

Mathematical modeling

Derivation of the kinetic equation

To describe the dynamics of the serial dilution experiment, we derive a simple ODE model. We consider a contest with two strategies, *A* and *B*. The payoffs are given by the matrix:

	A	*B*
A	*a*	*b*
B	*c*	*d*

In our context all entries are positive: $a, b, c, d > 0$.

We use the following variables: x_0 is the concentration of the *A* precursor (**WXY**), y_0 is the concentration of the *B* precursor (**WXY**), z denotes the concentration of the **Z** molecule, x_1 is the complex formed between the A precursor and Z, y_1 is the complex formed between the B precursor and **Z**. The variables x and y denote the concentration of the *A* and *B* molecule (**WXYZ**), respectively.

In the dilution experiment, the two precursor molecules and the **Z** molecule are provided at constant level, and the complex is formed in a reversible chemical reaction

$x_0 + z \rightleftharpoons x_1$
$y_0 + z \rightleftharpoons y_1$

Thus, x_1 and y_1 are also provided at constant level, and they give rise to the respective **WXYZ** molecule according to the catalyzed reactions

$x_1 \overset{ax}{\rightarrow} x$
$x_1 \overset{by}{\rightarrow} x$
$y_1 \overset{cx}{\rightarrow} y$
$y_1 \overset{dy}{\rightarrow} y$

Therefore, the kinetic equation (that would occur in a flow reactor) is

$$\dot{x} = (ax + by)x_1 - \phi x$$
$$\dot{y} = (cx + dy)y_1 - \phi y, \qquad \textbf{[3]}$$

Here ϕ is a parameter chosen such that the concentration of *A* and *B* is constant, $x + y = C$ and $\dot{x} + \dot{y} = 0$. Without loss of generality, we can set C=1 (we only need to replace the variables x and y by the transformed variables x/C and y/C). In that case, ϕ can be calculated as

$\phi = (ax + by)x_1 + (cx + dy)y_1$.

Moreover, since x_1 and y_1 are provided at equal concentrations, we may set $x_1 = y_1 = 1$. This may lead to a change of the time scale, but it leaves the trajectories of Eq. **[3]** unchanged. Thus, the dynamical equation simplifies to

$$\dot{x} = ax + by - \phi x$$
$$\dot{y} = cx + dy - \phi y, \qquad \textbf{[1]}$$

with $\phi = (a + c)x + (b + d)y$.

Properties of the dynamical equation

In the following, we list a few interesting properties of the dynamical equation.

Property 1.
The dynamical equation **[1]** has a unique and globally stable equilibrium $(\hat{x}, \hat{y})$ with $0 < \hat{x}, \hat{y} < 1$ and $\hat{x} + \hat{y} = 1$. In the generic case that $a + c \neq b + d$, the equilibrium frequency of $\hat{x}$ is given by

[2] $$\hat{x} = \frac{a-2b-d+\sqrt{(a-d)^2+4bc}}{2(a+c-b-d)}.$$

Otherwise, if $a + c = b + d$, the equilibrium frequency is $\hat{x} = b/(b + c)$.

Proof. Since $x + y = 1$, the first equation in **[1]** can be written as

$$\dot{x} = ax + b(1 - x) - \phi x = b + (a - 2b - d)x - (a + c - b - d)x^2 =: f(x).$$

The function $f(x)$ has the unique zero $\hat{x}$ in the unit interval (0,1). Since $f(0) = b > 0$, it follows that $f(x) > 0$ when $0 \leq x < \hat{x}$, whereas $f(x) < 0$ when $\hat{x} < x \leq 1$. Therefore, for any given initial frequency x, orbits converge towards $\hat{x}$. □

Let us next explore how the position of the equilibrium is affected by the entries of the payoff matrix. The following results follow directly from Eq. **[2]**.

Property 2.
1. The equilibrium frequency $\hat{x}$ is strictly increasing in a and b, and strictly decreasing in c and d.
2. All other parameters unchanged, $a \to \infty$ or $b \to \infty$ implies $\hat{x} \to 1$, whereas $c \to \infty$ or $d \to \infty$ implies $\hat{x} \to 0$.
3. The equilibrium frequency satisfies $\hat{x} = 1/2$ if and only if $a + b = c + d$. Similarly, it satisfies $\hat{x} > 1/2$ if and only if $a + b > c + d$.

As a consequence of the previous result, we can also draw the following connection between the equilibrium frequency and the type of game considered.

Property 3.
1. In a Dominance or Counter-Dominance scenario, $\hat{x} > 1/2$ if and only if it is A that dominates B.
2. In a Selfish scenario, $\hat{x} > 1/2$ if and only if A risk-dominates B.
3. In a Cooperation scenario, $\hat{x} > 1/2$ if and only if A is also played with higher frequency in the symmetric Nash equilibrium.

Dynamical equation for $n \times n$ constests

To describe the dynamics of the rock-paper-scissors contest, we generalize the previous dynamical equation to arbitrary $n \times n$ contests. Let $M = (m_{ij})$ be the payoff matrix of such a contest, and let $x = (x_1, \cdots, x_n)^T$ be the vector that gives the frequency of each **WXYZ** molecule, such that $x_1 + \cdots + x_n = 1$. Then the n-strategy analogue of Eq. **[1]** is

[4] $$\dot{x} = Mx - \phi x,$$

with $\phi = \sum_{i,j} m_{ij} x_j$. Equation **[4]** can be considered as a slightly generalized version of the quasi-species equation. It has a unique fixed point in the interior of the state space, which is globally stable. The fixed point can be found by solving the eigenvector problem $Mx = \lambda x$, where λ is the largest eigenvalue of M. The theorem of Perron and Frobenius for positive matrices guarantees that the corresponding normalized eigenvector x is unique, and that all entries of x are positive.

In the following, let us summarize a few simple properties of the dynamical equation **[4].**

Property 4.

1. The unit simplex $\Delta = \{x \in \mathbb{R}^n \mid x \geq 0, x_1 + \cdots + x_n = 1\}$ is invariant under the dynamical equation **[4]**; that is, if the initial state $x(0) \in \Delta$ then $x(t) \in \Delta$ for all times *t*.
2. The edges of the unit simplex are not invariant under the dynamics in **[4]**; if $x_i = 0$ then $\dot{x}_i > 0$.

Proof. The sum of all entries of x does not change over time, due to our choice of ϕ. Moreover, if $x_i = 0$, then it follows from Eq. **[4]** that $\dot{x}_i = (Mx)_i - 0 > 0$.

The previous result points to an important difference between the dynamical equation **[4]** and replicator dynamics (see also Fig. S7). Replicator dynamics is *non-innovative* – if a strategy is initially absent, then the evolutionary dynamics does not introduce this strategy at some later time point. In contrast, the kinetic dynamics described in **[4]** predicts that absent **WXYZ** strategies are introduced immediately, due to the catalytic effect of the other **WXYZ** molecules (provided that the required precursor **WXY** for the absent strategy is available).

Next, let us describe the relationship between the Nash equilibria of a contest with payoff matrix *M*, and the unique equilibrium of the kinetic equation **[4]**.

Property 5.
Let $M = (m_{ij})$ be the payoff matrix of an *n*-strategy contest, and let $x = (x_1, \cdots, x_n)^T$ be the unique equilibrium of Eq. **[4]**. Then the following are equivalent:

1. x is a Nash equilibrium.
2. The equilibrium is in the center of the simplex, $x = (1/n, \cdots, 1/n)^T$.
3. The row sums of *M* coincide, $m_{i1} + \cdots + m_{in} = m_{j1} + \cdots + m_{jn}$ for all $1 \leq i, j \leq n$.

Proof.

$1 \Rightarrow 2$. As x is a Nash equilibrium in the interior of the state space, all strategies yield the same expected payoff,

$$(Mx)_i = (Mx)_j \text{ for all } 1 \leq i, j \leq n.$$

Moreover, since x is the fixed point of Eq. **[4]**, and hence the eigenvector of M corresponding to some real eigenvalue $\lambda > 0$, it follows that

$$\lambda \cdot x_i = (Mx)_i = (Mx)_j = \lambda \cdot x_j.$$

In particular, $x_i = x_j$ for all $1 \leq i, j \leq n$, and thus $x = (1/n, \cdots, 1/n)^T$.

$2 \Rightarrow 3$. As $Mx = \lambda x$ for some $\lambda > 0$ and for $x = (1/n, \cdots, 1/n)^T$, it follows that

$$\frac{1}{n}(m_{i1} + \cdots + m_{in}) = \lambda/n \text{ for all } 1 \leq i \leq n.$$

Since the right hand side does not depend on *i*, neither does the left hand side. Therefore,

$$m_{i1} + \cdots + m_{in} = m_{j1} + \cdots + m_{jn} \text{ for all } 1 \leq i, j \leq n.$$

$3 \Rightarrow 1$. If the row sums of M coincide, it is easy to check that $x = (1/n, \cdots, 1/n)^T$ is the unique fixed point of Eq. **[4]**. In this fixed point, $(Mx)_i = (Mx)_j$ for all $1 \leq i, j \leq n$, and hence x is a Nash equilibrium. □

The previous result shows that in general, the kinetic equilibrium of Eq. **[4]** is not a Nash equilibrium – the only exception occurs when all rows of the payoff matrix sum up to the same value.

Discussion of the utility of game theory at the chemical level

Given the concordance between our experimental results and the ODE models that we constructed, the game-theoretic analysis appears to be a natural consequence of chemical kinetics, but kinetics viewed in an entirely new way. Our formalism allows us to summarize the dynamics between two genotypes in a single matrix, whose values can easily be interpreted. One only needs to know this matrix to calculate genotype equilibria. The dynamics can be interpreted using frequency-dependent selection. Each step along this analytical process is performed exactly as in evolutionary game theory, although the applied equilibrium concepts differ.

Put another way, game theory adds to the ability to assess rapidly the evolutionary outcomes of contests among pre-biotic genotypes such as RNA. Specifically it can allow one to understand how two *general* outcomes arise (dominance *vs*. co-existence), but more importantly, which *specific* mechanism is operational in any given situation: auto- and/or cross-catalysis. The Counter-dominance situation is a good example of this. An ODE analysis on its own would tell you that one genotype would rise to a high frequency at the expense of the other, but the specific mechanism for this – the receipt of greater cross-assembly benefits than self-assembly benefits – may be obscured. The 2x2 payoff matrix reveals this dynamic quickly and allows insight into the precise molecular events that underlie the evolutionary dynamics. The Prisoner's Dilemma has been biologically demonstrated in viruses (8) and yeast (9, 10), and we now demonstrate it at the raw (bio)chemical level.

In many environments envisaged for plausible conditions for the origin of life, there is a steady-state flux of resources or energy. Examples include, but are not limited to, thermal gradients leading to thermophoresis (11, 12), streams flowing downhill absorbing leaching chemical precursors (13, 14), and sporadically-fed aqueous pools (15). In these situations, nascent reproducing molecules would have had to compete for common resources, and our molecular experiments and model were designed to capture these characteristics, targeting a "pre-Darwinian" description of molecular evolution (*e.g*., 16, 17). The chemical game theoretic treatment allows an extention of the benefits of traditional evolutionary game theory down to a simpler, pre-life level.

With these parallels, we propose that game theory is applicable to the events leading to the chemical origins of life. Intermolecular interactions, driven mainly by non-covalent bonding strengths, can be hypothesized as giving rise to a build-up of network complexity among prebiotic polymers as has been discussed for other RNAs (18), proteins (19), and lipids (20). Here we have provided an empirical example of how game-theoretic patterns can be manifest in a chemical system, and one that has prebiotic relevance. While the dynamics of chemical reproducers can be described in terms of classical ODE equations, the game-theoretic construct gives insight as to what happens when one goes from a small number of nodes in a network to a larger number of nodes.

Although one needs to be wary of over-interpretation, game theory at the chemical level allows for a clear evolutionary perspective of prebiotic dynamics. From a practical standpoint, what we have shown is that from knowing the influence on catalysis of a single nucleotide-pair interaction – here the middle nucleotide of the IGS-tag triplet, akin to the middle position in a codon-anticodon pairing – on catalysis, one could predict general outcomes from contests among a small number of competitors vying for a shared resource. Note that in the predicted Cooperation competitions – those leading to significant steady-state frequencies of both genotypes – none of the participating genotypes has a Watson-Crick pair between their M and N nucleotides. The presence of a non-canonical nucleotide pair in the IGS-tag recognition process leads to the situation where the off-diagonal terms in the payoff matrix (*b* and *c*) are greater than the diagonal terms (*a* and *d*), thereby promoting a type of molecular cooperation (21), in that molecules are forced kinetically to forego some of their reproductive potential to assemble others (22). In the converse case, the Selfish scenario, the diagonal terms in the matrix exceed the off-diagonal terms, leading also to co-existence, but one achieved in the opposite manner. (The CG *vs*. AU game is perhaps the most extreme example of a Selfish scenario, and while the CG self-assembly rate constant exceeds that of AU by only 30%, we predict that the steady-state frequency of CG should reach 96% even with a continual supply of equimolar AU; see Fig. S4.)

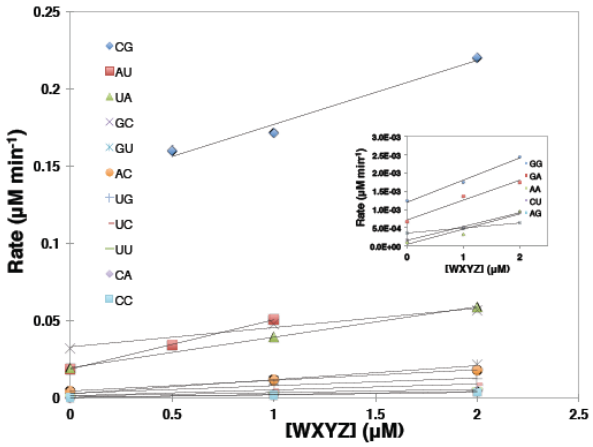

Table 1. Rate constants, k_a (min^{-1}), for the 16 genotype variations of WXY.

Genotype	k_a (min^{-1})	Std. error	r^2
CG	0.0415	0.0066	0.98
AU	0.0319	0.0011	1.00
UA	0.0197	0.0004	1.00
GC	0.0125	0.0021	0.97
GU	0.0091	0.0007	0.99
AC	0.0069	0.0002	1.00
UG	0.0049	0.0004	0.99
UC	0.0038	0.0002	1.00
UU	0.0022	0.0001	1.00
CA	0.0020	0.0000	1.00
CC	0.0016	0.0001	1.00
GG	0.0006	0.0001	0.99
GA	0.0005	0.0001	0.98
AA	0.0004	0.0001	0.92
CU	0.0004	0.0000	1.00
AG	0.0001	0.0000	0.99

Supplementary Figure 1. Calculation of self-assembly autocatalytic rate constants. Left: raw data for the rates of self-assembly for the 16 genotypes $_{GMG}$**WXY**$_{CNU}$, where M and N are free to vary. Rates were measured by doping in 0 μM, 0.5 μM, 1 μM, or 2 μM full-length **WXYZ** into reactions containing 1 μM $_{GMG}$**WXY**$_{CNU}$ and 1 μM **Z** as described in ref. (2) and the Methods above. Each point represents the average of three independent trials. Main plot: data for the 11 fastest self-assembling genotypes, where rates were measured for reaction times of 5 minutes or less. Inset: data for the five slowest self-assembling genotypes, where rates were measured for reaction times of 10 minutes or less. Right: Table (with r^2 linear regression values included) that depicts the computed autocatalytic rate constants (k_a) via the means described above (2), based on the method of von Kiedrowski (7).

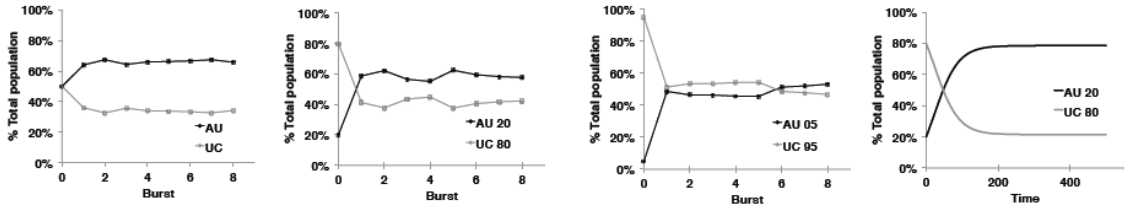

Supplementary Figure 2. Variation of the initial frequencies in the AU *vs*. UC contest. From left to right, the initial **WXY** molar frequencies are AU:UC:50:50 (experimental), AU:UC:20:80 (experimental), AU:UC:5:95 (experimental), and AU:UC:20:80 (model). All experiments converge on similar final equilibrium concentrations, with AU > UC (but not exclusionary), as predicted by the model. Note, in this 2-strategy contest, the chemical outcome (Selfish) is an analog of the Stag Hunt biological game scenario. In biological evolutionary competitions, the Stag Hunt scenario is a bi-stable one, in which the final outcome is heavily dependent on the initial conditions, with a definable tipping point. Such bi-stability is not observed in these experiments, highlighting a key difference between biological games based on replication and chemical games based on reproduction (assembly). See main text for more discussion.

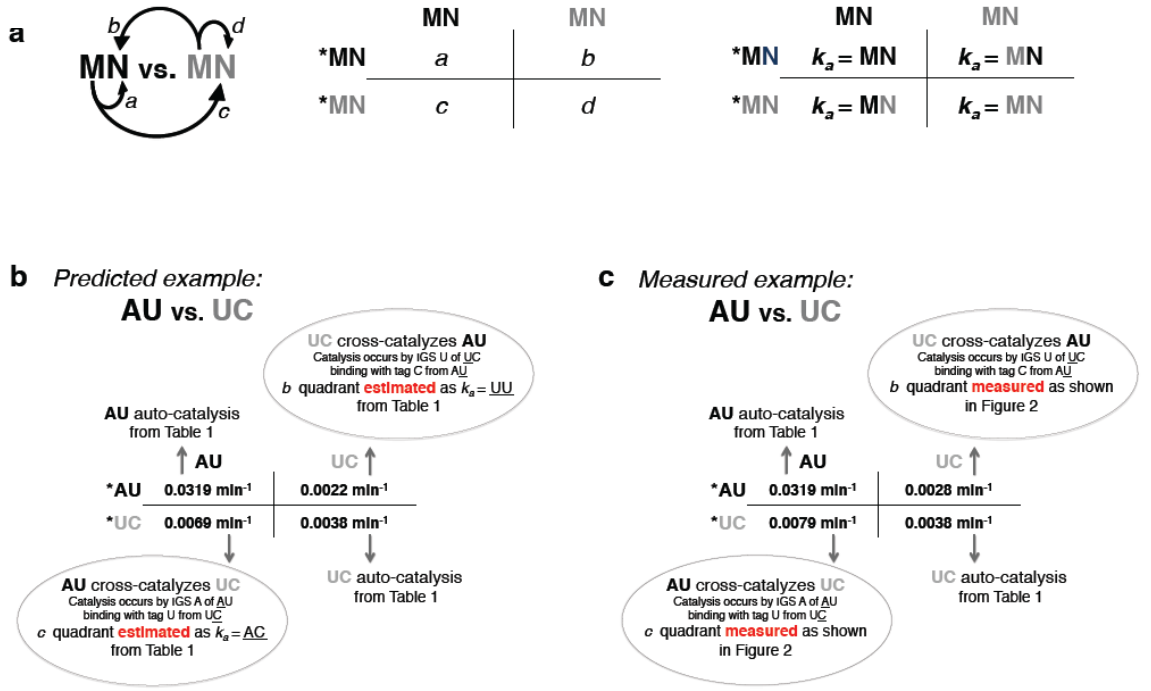

Supplementary Figure 3. Use of IGS and tag nucleotides to predict 2-strategy outcomes. Here the logic for the construction of the predicted 2x2 payoff matrices is explained. (**a**) A depiction of how the MN notation translates into the *a*, *b*, *c*, and *d* values in the payoff matrix. The *a* and *d* values (diagonal terms) are data taken from the empirical self-assembly experiments tabulated in the Table in Fig S1. (**b**) and **(c)** An example game of AU *vs*. UC is shown. The *a* value is the self-assembly autocatalytic rate constant that results when $_{GAG}$**WXY**$_{CUU}$ is incubated with **Z**. This reaction is determined by the strength of a A-U nucleotide pair within the interaction between an IGS triplet in one RNA fragment and the "tag" in another (Fig. 1*C*). Likewise the *d* value is the self-assembly autocatalytic rate constant that results when $_{GUG}$**WXY**$_{CCU}$ is incubated with **Z**. On the other hand, the *b* and *c* values (off-diagonal terms) can be derived in two different manners. They can either be *estimated* using the appropriate nucleotide-pair value from the Table in Fig. S1 (panel **c**), or they can be *measured* using an experimental competition between two **WXY** genotypes as shown in Fig. 2 (panel **b**). Using *estimated* values of *b* and *c*, we have predicted the outcomes of all 72 contests in which no values are predicted to be equal (Fig. S4). For example, the AU *vs*. UC contest is predicted to give a Selfish outcome by this method, as shown. In all panels, the asterisk (*) here denotes that in a 2-genotype interaction, the payoff is to the row player in competition with the column player, and using the differential ^{32}P-labeling technique (Fig. 2A), we can track the rate of assembly of single genotypes in a mixture.

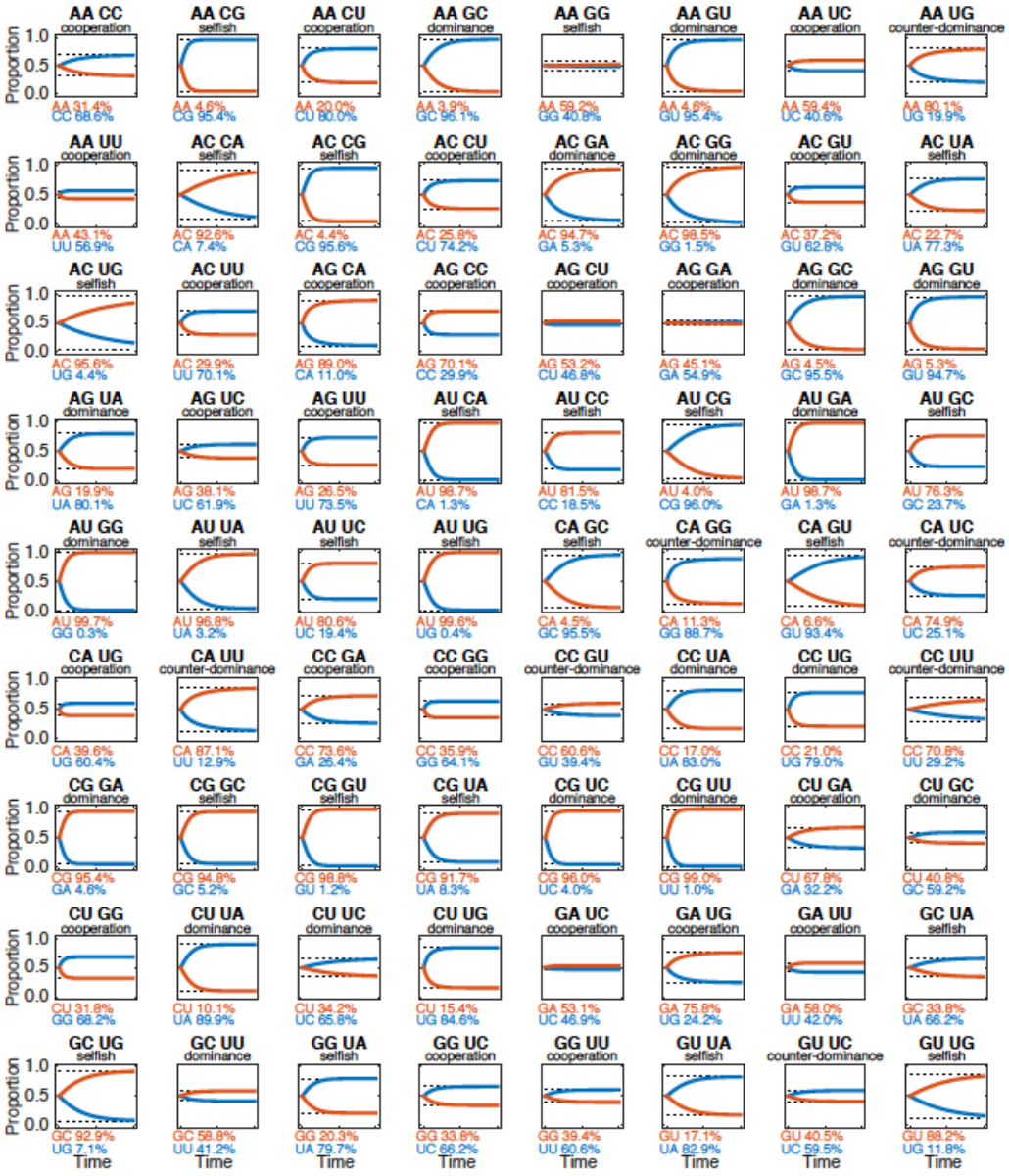

Supplementary Figure 4. Plots of outcomes of all 72 strict 2-strategy contests from predicted self-assembly matrices. By eliminating cases with equal payoffs (*e.g.*, AU *vs*. AC; Fig. S5), there are 72 possible such contests. The predictions are that 26% of the scenarios should lead to the Dominance, 32% to the Cooperation, 32% to the Selfish, and 10% to the Counter-dominance outcomes (Fig. S4). It is important to realize that the Dominance and Counter-dominance scenarios occasionally lead to fairly high frequencies of the "losing" genotype (*e.g.*, 30% UU, in CC *vs*. UU; Fig. S4). Conversely the two co-existence scenarios can sometimes lead to the near fixation of one genotype (*e.g.*, CG in CG *vs*. GU). These cases are the exceptions to the rule however, and are a consequence of the steady-state nature of both the experiments and modeling where the Z resource is continually replenished. Each panel shows the expected 2-strategy dynamics, for all 72 payoff matrices that can be derived from the self-assembly data in the Table in Fig. S1. For details on how these matrices were obtained, see Fig. 2*B* and Fig. S3. These matrices were then used as our input to calculate the expected dynamics according to the kinetic equation **[1]** above. As this figure suggests, different 2-strategy contests can have remarkably different dynamics, even if the contests are taken from the same game class. The predicted equilibrium frequencies according to equation **[2]** above are depicted by the dotted black lines. Exact equilibrium frequencies are provided at the bottom of each panel.

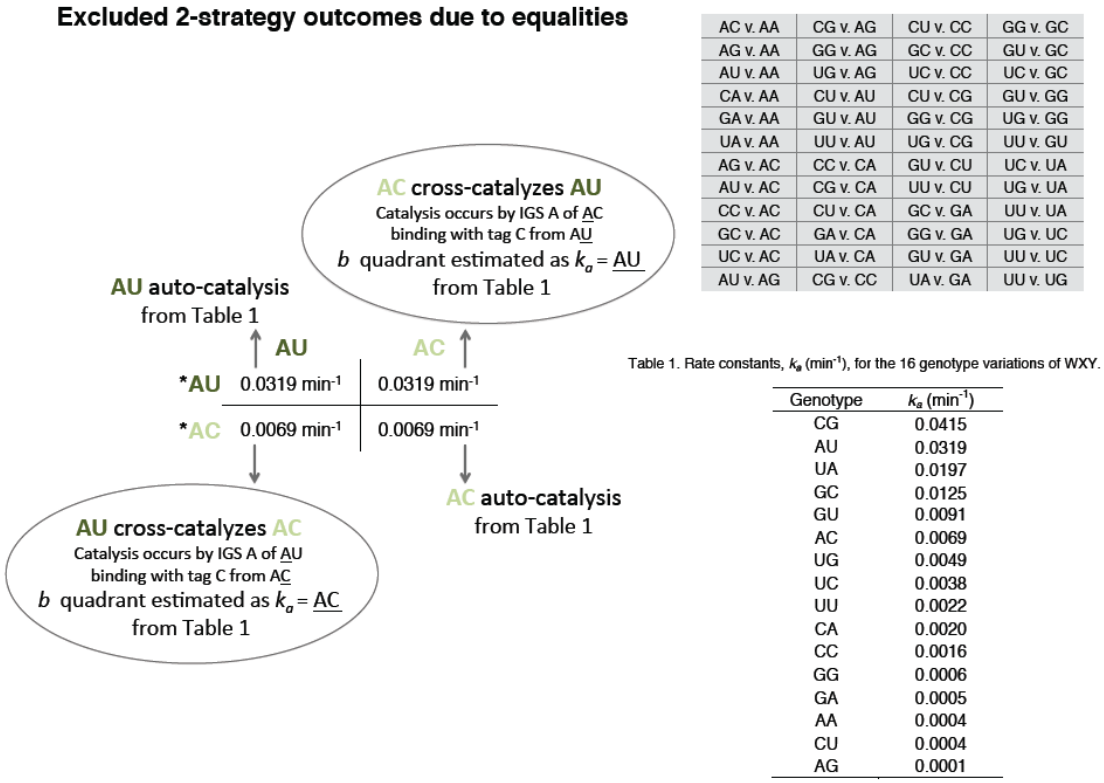

Table 1. Rate constants, k_a (min^{-1}), for the 16 genotype variations of WXY.

Genotype	k_a (min^{-1})
CG	0.0415
AU	0.0319
UA	0.0197
GC	0.0125
GU	0.0091
AC	0.0069
UG	0.0049
UC	0.0038
UU	0.0022
CA	0.0020
CC	0.0016
GG	0.0006
GA	0.0005
AA	0.0004
CU	0.0004
AG	0.0001

Supplementary Figure 5. Tabluation of the 48 2-genotype contests that generate predicted equal values in their 2x2 payoff matrices. There are 16(15)/2 = 120 distinct 2-strategy contests from 16 **WXY** genotypes, but 48 of these will generate values in the predicted payoff matrix that are *equal*, using the logic shown here. When two genotypes compete with the same M or N nucleotide, then the self-assembly values (Table) will predict two identical values in the matrix. For example, when AU competes *vs*. AC as shown here, the *a* and *b* values in the matrix both would derive from the AU self-assembly rate constant value in the Table, which is 0.0319 min^{-1}. The *a* value represents an A-U pairing during the catalytic self-assembly of $_{GAG}$**WXY**$_{CUU}$ and **Z**, while the *b* value represents an A-U pairing during the catalytic cross-assembly of $_{GAG}$**WXY**$_{CUU}$ and **Z** by a $_{GAG}$**WXY**$_{CCU}$-containing ribozyme. Likewise in this particular contest, the *c* and *d* values would be predicted to be equal. Equal values in the payoff matrix do not lead to strict equilibria. Thus for the purposes of forecasting outcomes from all possible 2-strategy contests using only self-assembly data, these 48 cases are excluded, leaving 72 possible contests, as shown in Fig. S4. Again, the asterisk (*) here denotes that in a 2-genotype interaction, the payoff is to the row player in competition with the column player, and using the differential ^{32}P-labeling technique (Fig. 2A), we can track the rate of assembly of single genotypes in a mixture.

a **3 x 3 experimental matrix**

	UC	AA	GU
UC	0.0038	0.0182	0.0560
AA	0.0504	0.0004	0.0005
GU	0.0037	0.0312	0.0091

b **Three 2 x 2 experimental matrices**

	UC	AA
UC	0.0038	0.0182
AA	0.0504	0.0004

c > b > a > d
cooperation

	GU	AA
GU	0.0091	0.0312
AA	0.0005	0.0004

b > a > c > d
dominance

	GU	UC
GU	0.0091	0.0037
UC	0.0560	0.0038

c > a > d > b
counter-dominance

Supplementary Figure 6. Predicted 3x3 payoff matrix in the 3-strategy contest between UC, AA, and GU (Fig. 4). (**a)** The 3x3 matrix, compiled from two sources (in analogy to Fig. 2*B*). The diagonal terms (0.0038, 0.0004, and 0.0091) were self-assembly autocatalytic rate constants from the Table in Fig. S1. The off-diagonal terms were collected from the appropriate off-diagonal terms measured in individual 2-strategy contests shown in panel (**b**). For example, the value 0.0504 (first column, second row) in the 3x3 matrix derives from the measured value of *c* in the 2x2 matrix for the UC *vs*. AA contest. A stable interior equilibrium point is predicted to exist (23, 24). This was in fact seen in the experiment (Fig. 4*A*), and the scenario is thus a chemical form of Rock-Paper-Scissors (RPS). Because one pairwise interaction (UC *vs*. AA) in this context results not in pure dominance, but Cooperation, the present contest is technically a weak form of a RPS, in the sense that every strategy can invade the previous strategy, and it can be invaded by the next strategy (see Fig. S7). In our system with only 16 possible genotypes that are roughly binary in their interactions with other genotypes (Watson-Crick base pairing in the M-N interaction or not), it is not possible to construct a strictly strong RPS scenario, because at least one pairwise interaction will not be a dominance scenario. With this matrix analysis, one can see a more general connection to network evolution. The values in the payoff matrix are equivalent to the weights of the connections in a network, and the sum of the weighted paths in a network gives an approximation of the dominant eigenvector x_i (the steady-state frequencies of each of *i* species in a network). See reference (25) for more discussion of this point.

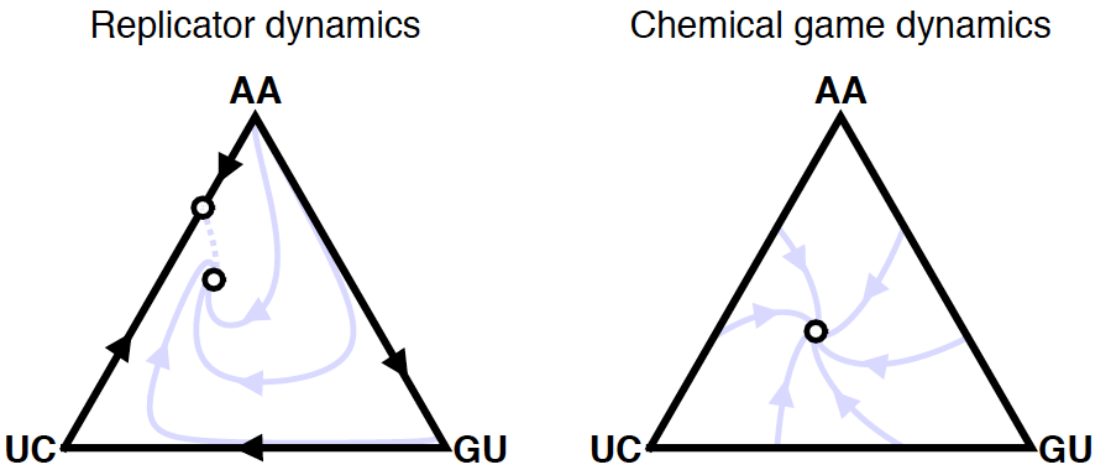

Supplementary Figure 7. Comparison of biological (replicator) dynamics with the chemical game dynamics. Based on the 3x3 experimental matrix displayed in Fig. S6, the two graphs show the resulting replicator dynamics (left) and the dynamics according to the kinetic equation **[4]** above (right). Replicator dynamics predicts cyclical behavior: AA can be invaded by GU, GU can be invaded by UC, and UC in turn can be invaded by AA. The fixed point on the edge between UC and AA is unstable, and all orbits spiral towards the unique Nash equilibrium in the interior of the state space (with equilibrium proportions UC 35.8%, AA 50.4%, GU 13.8%). However, in the kinetic equilibrium (right), AA is considerably less abundant than predicted by the Nash equilibrium (UC 39.1%, AA 35.0%, GU 25.8%). Moreover, in the right graph, the edges of the Simplex are no longer invariant because absent strategies are introduced continually (as described in detail in the *Mathematical Modeling* section above).

Kruskal-Wallis test

Game	H	Critical value	P value
dominance CG vs. GA	7.821	6.897436	0.046
dominance GU vs. AA	9.359	6.897436	0.025
cooperation AC vs. UU	8.504	8.435897	0.009
cooperation UC vs. AA	10.385	6.897436	0.016
selfish AU vs. UC	10.385	8.435897	0.009
counter-dominance CA vs. GG	9.667	8.435897	0.009
counter-dominance GU vs. UC	8.197	6.897436	0.042

Supplementary Figure 8. Statistical tests for ordinal rankings. The Kruskal-Wallis non-parametric test was used to test the statistical significance of the rank order of the values in the 2x2 payoff matrices. The seven 2-strategy contests depicted in Fig. 2 were analyzed in this fashion, using the variation in empirical data provided by the three independent replicates of the experiments. The test statistic *H* was computed as per Sokal and Rohlf (26) and compared to the critical values provided by Meyer and Seaman (27) from the exact probability distribution. All rank-order values for these games were statistically significant at the $P < 0.05$ value or better.

References for Supplementary Information

1. Reinhold-Hurek B, Shub DA (1992) Self-splicing introns in tRNA genes of widely divergent bacteria. *Nature* 357:173–176.
2. Hayden EJ, von Kiedrowski G, Lehman N (2008) Systems chemistry on ribozyme self-construction: Evidence for anabolic autocatalysis in a recombination network. *Angew Chem Int Ed* 47:8424–8428.
3. Kuo LY, Davidson LA, Pico S (1999) Characterization of the *Azoarcus* ribozyme: tight binding to guanosine and substrate by an unusually small group I ribozyme *Biochim Biophys Acta* 1489:281–292.
4. Hayden EJ, Lehman N (2006) Self-assembly of a group I intron from inactive oligonucleotide fragments. *Chem Biol* 13:909–918.
5. Riley CA, Lehman N (2003) Generalized RNA-directed recombination of RNA. *Chem Biol* 10:1233–1243.
6. Vaidya N, Manapat ML, Chen IA, Xulvi-Brunet R, Hayden EJ, Lehman N (2012) Spontaneous network formation among cooperative RNA replicators. *Nature* 491:72–77.
7. von Kiedrowski G (1986) A self-replicating hexadeoxynucleotide. *Angew Chem Int Ed Engl* 25:932–935.
8. Turner PE, Chao L (1999) Prisoner's dilemma in an RNA virus. *Nature* 398:441–443.
9. Frick T, Schuster S (2003) An example of the prisoner's dilemma in biochemistry. *Naturwissenshaften* 90:327–331.
10. Van Dyken JD, Müller MJI, Mack KML, Desai MM (2013) Spatial population expansion promotes the evolution of cooperation in an experimental Prisoner's Dilemma. *Curr Biol* 23:919–923.
11. Baaske P, Weinert FM, Duhr S, Lemke KH, Russell MJ, Braun D (2007) Extreme accumulation of nucleotides in simulated hydrothermal pore systems. *Proc Natl Acad Sci USA* 104:9346–9351.
12. Mast CB, Schink S, Gerland U, Braun D (2013) Escalation of polymerization in a thermal gradient. *Proc Natl Acad Sci USA* 110:8030–8035.
13. Benner SA, Kim H-J, Carrigan MA (2012) Asphalt, water, and the prebiotic synthesis of ribose, ribonucleotides, and RNA. *Acc Chem Res* 45:2025–2034.
14. Patel BH, Percivalle C, Ritson DJ, Duffy CD, Sutherland JD (2015) Common origins of RNA, protein and lipid precursors in a cyanosulfidic protometabolism. *Nature Chemistry* 7:301–307.
15. Yarus M (2012) Darwinian behavior in a cold, sporadically fed pool of ribonucleotides. *Astrobiology* 12:870–883.
16. Nowak MA, Ohtsuki H (2008) Prevolutionary dynamics and the origin of evolution. *Proc Natl Acad Sci USA* 105:14924–14927.
17. Arnoldt H, Strogatz SH, Timme M (2015) Switching between distributed species state in a simple model of early life. *Phys Rev E* 92:052909.
18. Lincoln TA, Joyce GF (2009) Self-sustained replication of an RNA enzyme. *Science* 323:1229–1232.
19. Ashkenasy G, Jagasia R, Yadav M, Ghadiri MR (2004) Design of a directed molecular network. *Proc Natl Acad Sci USA* 101:10872–10877.
20. Segré D, Ben-Eli D, Lancet D (2000) Compositional genomes: Prebiotic information transfer in mutually catalytic noncovalent assemblies. *Proc Natl Acad Sci USA* 97:4112–4117.
21. Higgs PG, Lehman N (2015) The RNA world: Cooperation and conflict at the origins of life. *Nature Rev Genet* 16:7–17.
22. Nowak MA (2006) Five rules for the evolution of cooperation. *Science* 314:1560–1563.
23. Nowak MA (2006) *Evolutionary Dynamics: Exploring the Equations of Life* (Belknap Press of Harvard, Cambridge, MA).
24. Nowak MA, Sigmund K (2004) Evolutionary dynamics of biological game. *Science* 303:793–799.
25. Nghe P, Hordijk W, Kauffman SA, Walker SI, Schmidt FJ, Kemble H, Yeates JAM, Lehman N (2015) Prebiotic network evolution: six key parameters. *Mol BioSyst* 11:3206–3217.
26. Sokal RR, Rohlf FJ (1981) *Biometry: The Principles and Practice of Statistics in Biological Research.* (W. H. Freeman & Co., New York, NY).
27. Meyer JP, Seaman MA *Expanded Kruskal-Wallis Tables*, downloaded on 1July2015 from http://faculty.virginia.edu/kruskal-wallis/.